PHYSICAL REVIEW D **84,** 013011 (2011)

Tribimaximal mixing from small groups

Krishna Mohan Parattu[*]
Inter-University Centre for Astronomy and Astrophysics, Ganeshkhind, Pune 411007, India

Akın Wingerter[†]
Laboratoire de Physique Subatomique et de Cosmologie UJF Grenoble 1, CNRS/IN2P3, INPG, 53 Avenue des Martyrs, F-38026 Grenoble, France
(Received 9 May 2011; published 26 July 2011)

Current experimental data on the neutrino parameters are in good agreement with tribimaximal mixing and may indicate the presence of an underlying family symmetry. For 76 flavor groups, we perform a systematic scan for models: The particle content is that of the standard model plus up to three flavon fields, and the effective Lagrangian contains all terms of mass dimension ≤ 6. We find that 44 groups can accommodate models that are consistent with experiment at 3σ, and 38 groups can have models that are tribimaximal. For $A_4 \times \mathbb{Z}_3$, T_7, and T_{13} we look at correlations between the mixing angles and make a prediction for θ_{13} that will be testable in the near future. We present the details of a model with $\theta_{12} = 33.9°$, $\theta_{23} = 40.9°$, $\theta_{13} = 5.1°$ to show that the recent tentative hints of a nonzero θ_{13} can easily be accommodated. The smallest group for which we find tribimaximal mixing is T_7. We argue that T_7 and T_{13} are as suited to produce tribimaximal mixing as A_4 and should therefore be considered on equal footing. In the appendixes, we present some new mathematical methods and results that may prove useful for future model building efforts.

DOI: 10.1103/PhysRevD.84.013011 PACS numbers: 14.60.Pq

I. INTRODUCTION

Neutrino physics is a fast developing field. The past decade has seen the discovery of neutrino masses [1,2] and ever improving measurements of the neutrino mixing matrix U_{PMNS} [3,4]. Our growing knowledge of the neutrino parameters [5,6] has almost raised more questions than it has answered: Why are neutrinos so light? Why are two of the mixing angles large and one vanishingly small? Why is U_{PMNS} so different from U_{CKM} [7]? These are some of the questions that any model for the neutrino sector needs to address.

Experimental data suggest that the mixing angles are in good agreement with tribimaximal mixing (TBM) [8,9]. The very form of the Harrison-Perkins-Scott matrix U_{HPS} is suggestive of an underlying family symmetry between the three generations of leptons. In the past years, much effort has been vested in finding a family symmetry that would naturally lead to tribimaximal mixing, and to that end, some 20 odd groups have been the subject of model building efforts (see Refs. [10–12] and references therein).

It has been argued that A_4 is particularly relevant for producing tribimaximal mixing [13–16], and by the number of publications (see e.g. Table 2 in Ref. [10]), it is certainly the most popular discrete symmetry used for model building. That is why we start out by following the same path to construct all $A_4 \times \mathbb{Z}_3$ models with up to three flavon fields, where the lepton doublet L transforms as a triplet. We find 22 932 inequivalent models, of which 4481 (19.5%) give mixing angles that are consistent with experiment at 3σ, and 4233 (18.5%) that are tribimaximal. Restricting θ_{12} and θ_{23} to their respective 3σ intervals, we obtain an interesting prediction for θ_{13} whose value is currently not known with very high precision: By far, the most likely value is $\theta_{13} = 0°$, and there are extremely few models for $0° \lneq \theta_{13} \lesssim 12°$. We also present a model where all three mixing angles, $\theta_{12} = 33.9°$, $\theta_{23} = 40.9°$, and $\theta_{13} = 5.1°$, lie in their respective 1σ intervals to show that it is possible to accommodate the recent tentative hints of a nonzero θ_{13} [6,17,18].

Next we explore whether A_4 is really special or we are looking for tribimaximal models "under the lamppost." There are 1048 groups with less than or equal to 100 elements, and 90 of them have a three-dimensional irreducible representation. For 76 groups, we construct all models with up to three flavon fields, where the lepton doublet L transforms in a three-dimensional irreducible representation. For the remaining 14 groups, a systematic scan would simply take too long. We find 44 groups (58%) that can accommodate models which are consistent with experiment at the 3σ level, and 38 groups (50%) that can produce tribimaximal mixing. The smallest group for which we find tribimaximal mixing is T_7, and the group with the largest fraction of tribimaximal models is T_{13}. Incidentally, for T_{13} (and the other metacyclic groups) the set of tribimaximal models and the set of 3σ models are almost identical, and this may be pointing towards a profound connection between T_{13} and tribimaximal mixing that is more pronounced as compared to A_4. For a

[*]krishna@iucaa.ernet.in
[†]akin@lpsc.in2p3.fr

recent publication that uses T_{13} for model building, see Ref. [19].

A systematic scan of discrete *Abelian* family symmetries has been performed before [20]. Our analysis is complementary in the sense that we only consider non-Abelian flavor groups that can have three-dimensional irreducible representations.

For our analysis, the computer algebra program GAP [21] played a central role. We used GAP to obtain the character table, the dimension of the conjugacy classes, and the explicit form of the representation matrices for the 76 groups that we considered in this publication. In contrast to e.g. solving renormalization group equations, the use of computers for algebraic and group theoretic operations is not widespread (a notable exception is Ref. [22]). We strongly advocate the use of the Small Groups Library [23] which collects, in one place, and provides easy access to all finite groups of order at most 2000 (except 1024).

In the appendixes we present some new developments and mathematical background information relevant for model building with discrete symmetries.

In Appendix A, we list the 90 groups of order less than or equal to 100 that have a three-dimensional irreducible representation. For each group, we indicate whether it is a subset of U(3), U(2), or U(2) $\times$ U(1) and, at the same time, check whether it contains A_4 as a subgroup. Because of its length, the full list of the 1048 groups of order at most 100 is presented in a separate file [24].

In Appendix B we give the full details on how we generated the 1048 groups and compiled the tables in Appendix A and Ref. [24]. We elaborate on some disagreement that we have with the existing literature.

In Appendix C, we discuss an algorithm due to van den Broek and Cornwell [25] for calculating the Clebsch-Gordan coefficients (CGCs) for any finite group. This allows us to construct the group invariants or, more generally, contract the family indices in the Lagrangian without referring to heuristic constructions as is common practice in the current literature.

II. EXPERIMENTAL CONSTRAINTS

The leptonic mixing matrix U_{PMNS} is generally parametrized by three angles, θ_{12}, θ_{23}, θ_{13}, and one Dirac phase, δ [26]. If the neutrinos are Majorana particles, there are two extra phases, ϕ_1 and ϕ_2, that do not affect neutrino oscillation phenomena [27] and are likely to remain unconstrained in the near future. In this paper, we use the standard parametrization [26] of U_{PMNS} except for the definition of the Majorana phases, where we follow Ref. [28]:

$$U_{\mathrm{PMNS}} = \begin{pmatrix} c_{12}c_{13} & s_{12}c_{13} & s_{13}e^{-i\delta} \\ -s_{12}c_{23} - c_{12}s_{13}s_{23}e^{i\delta} & c_{12}c_{23} - s_{12}s_{13}s_{23}e^{i\delta} & c_{13}s_{23} \\ s_{12}s_{23} - c_{12}s_{13}c_{23}e^{i\delta} & -c_{12}s_{23} - s_{12}s_{13}c_{23}e^{i\delta} & c_{13}c_{23} \end{pmatrix} \cdot \mathrm{diag}(e^{i\phi_1}, e^{i\phi_2}, 1). \quad (1)$$

For comparing our results from Sec. IV to experiment, we used Refs. [5,6,17]. In Table I, we summarize the relevant information for the reader's convenience.

The solar and atmospheric neutrino mixing angles, θ_{12} and θ_{23}, are relatively well determined. θ_{13}, on the other hand, effectively only has an upper bound. The experimental data are consistent with θ_{13} being zero, as e.g. in exact tribimaximal mixing. If $\theta_{13} = 0°$, the Dirac phase loses physical significance. Currently, there are possible hints for a nonzero θ_{13} [6,17,18]. A new generation of neutrino experiments will probe $\sin^2\theta_{13}$ down to about 10^{-2} [17].

TABLE I. The leptonic mixing angles from the global fit to data from Ref. [6] (first table, left column).

Parameter	Mean value	1σ range	3σ range
θ_{12}	34.4°	33.4°–35.4°	31.5°–37.6°
θ_{23}	42.8°	39.9°–47.5°	35.5°–53.5°
θ_{13}	5.6°	2.9°–8.6°	0°–12.5°

III. A PARADIGM: $A_4 \times \mathbb{Z}_3$ FAMILY SYMMETRY WITH THREE FLAVON FIELDS

To illustrate our general approach, we will choose $A_4 \times \mathbb{Z}_3$ as the family symmetry and reproduce the results of the now classic paper by Altarelli and Feruglio [16]. Here and in the following we will use the alternate notation C_n for $\mathbb{Z}_n$. Note that we could have taken any of the 439 820 models that we will be constructing in Sec. IV, but considering a model that is already well known has the advantage of a clearer presentation of our methodology by stressing the differences to other approaches.

The following lines of GAP code give us information on the group $A_4 \times C_3$:

```
1  group := SmallGroup(36, 11);;
2  Display (StructureDescription (group));
3  chartab := Irr(group);;
4  Display(chartab);
5  SizesConjugacyClasses (CharacterTable(group));
6  LoadPackage("repsn");;
7  for i in [1..Size(chartab)] do
```

```
8       rep := IrreducibleAffordingRepresentation(chartab[i]);
9       for el in Elements(group) do
10      Display(el^rep);
11      od;
12      od;
```

These lines can be entered directly at the GAP prompt or saved in a file and executed automatically as explained later. Line 1 defines the group in terms of its GAPID (see Appendix B 1). Lines 4 and 5 display the character table and the dimensions of the conjugacy classes, respectively. Finally, lines 6–12 give the explicit form of the matrices for all elements and for all representations of the group.

The first column of the character table gives the dimensions of the representations. We follow the common practice of denoting the representations by their dimensions and using primes or numbers to distinguish different representations of the same dimension:

$$\mathbf{1},\quad \mathbf{1}',\quad \mathbf{1}'',\quad \mathbf{1}''',\quad \mathbf{1}^{(4)},\quad \mathbf{1}^{(5)},\quad \mathbf{1}^{(6)},\quad \mathbf{1}^{(7)},\quad \mathbf{1}^{(8)},$$
$$\mathbf{3},\quad \mathbf{3}',\quad \mathbf{3}''. \tag{2}$$

Note that we deviate from the notation of Ref. [16], where the transformation properties of the representation under the factor subgroups are indicated, e.g. $\mathbf{3}\otimes\omega$, where ω is the primitive third root of unity. The reason why we choose another notation is that we would like to deal with all groups on equal footing. It is easy to establish the connection between the two notations by comparing the representation matrices of A_4 and $A_4\times C_3$, e.g. for the $\mathbf{3}$: The first, third, and fourth generators of $A_4\times C_3$ are identical to the three generators of A_4, and the second generator generates C_3. The explicit form for the generators of A_4 and $A_4\times C_3$ can be obtained by running the GAP script on the preceding page with the GAPIDs [12,3] and [36,11], respectively. We can now easily identify $\mathbf{3}\sim\mathbf{3}\otimes 1$, $\mathbf{3}'\sim\mathbf{3}\otimes\omega$, $\mathbf{3}''\sim\mathbf{3}\otimes\omega^2$. The other cases are handled in a completely analogous way (see Table II for the complete list). Strictly speaking, though, making this connection is not necessary.

The particle content of the model is given in Table II. In the following we list the terms that (i) are invariant under the standard model gauge symmetry, (ii) contain exactly two leptons, (iii) have mass dimension smaller than or equal to six, and (iv) are at most linear in the flavon vacuum expectation values (vevs):

$$LLh_uh_u\varphi_S,\quad LLh_uh_u\xi,\quad Leh_d\varphi_T,\quad L\mu h_d\varphi_T,\quad L\tau h_d\varphi_T. \tag{3}$$

To check invariance under the family symmetry we need the decomposition of tensor products into irreducible representations (see e.g. Ref. [29]) that is readily obtained from the character table and the dimensions of the conjugacy classes. For example, for the first term in Eq. (3) we have

TABLE II. Particle content and charges for the model given in Ref. [16]. The last column gives the family symmetry charges in our notation. In Ref. [16], there is an evident typo in the charge assignments to μ and τ in Sec. 4 as compared to Sec. 3 in the same publication.

Field	$\mathrm{SU}(2)_L\times\mathrm{U}(1)_Y$	A_4	C_3	$A_4\times C_3$
L	$(\mathbf{2},-1)$	$\mathbf{3}$	ω	$\mathbf{3}'$
e	$(\mathbf{1},2)$	$\mathbf{1}$	ω^2	$\mathbf{1}'$
μ	$(\mathbf{1},2)$	$\mathbf{1}''$	ω^2	$\mathbf{1}^{(8)}$
τ	$(\mathbf{1},2)$	$\mathbf{1}'$	ω^2	$\mathbf{1}^{(5)}$
h_u	$(\mathbf{2},1)$	$\mathbf{1}$	1	$\mathbf{1}$
h_d	$(\mathbf{2},-1)$	$\mathbf{1}$	1	$\mathbf{1}$
φ_T	$(\mathbf{1},0)$	$\mathbf{3}$	1	$\mathbf{3}$
φ_S	$(\mathbf{1},0)$	$\mathbf{3}$	ω	$\mathbf{3}'$
ξ	$(\mathbf{1},0)$	$\mathbf{1}$	ω	$\mathbf{1}''$

$$\begin{aligned}\mathbf{3}'\otimes\mathbf{3}'\otimes\mathbf{1}\otimes\mathbf{1}\otimes\mathbf{3}' &= (\mathbf{1}'+\mathbf{1}^{(5)}+\mathbf{1}^{(8)}+2\times\mathbf{3}'')\otimes\mathbf{3}'\\ &= 2\times\mathbf{1}+2\times\mathbf{1}'''+2\times\mathbf{1}^{(4)}+7\times\mathbf{3}.\end{aligned} \tag{4}$$

The tensor product contains two singlets and thus there are two ways to contract the family indices to obtain invariant combinations. To do this, however, we need to know the Clebsch-Gordan coefficients for $A_4\times C_3$, and to our surprise, the general method for the calculation of Clebsch-Gordan coefficients for any finite symmetry group is not well known. That is why we have dedicated Appendix C to discussing an algorithm [25] for the calculation of Clebsch-Gordan coefficients for finite groups. The first term in Eq. (3) after contracting the family indices becomes

$$\begin{aligned}&\frac{1}{\sqrt{3}}L_2L_3h_uh_u\varphi_{S,1}+\frac{1}{\sqrt{3}}L_3L_1h_uh_u\varphi_{S,2}\\ &+\frac{1}{\sqrt{3}}L_1L_2h_uh_u\varphi_{S,3}+\frac{1}{\sqrt{3}}L_1L_1h_uh_u\xi\\ &+\frac{1}{\sqrt{3}}L_2L_2h_uh_u\xi+\frac{1}{\sqrt{3}}L_3L_3h_uh_u\xi.\end{aligned} \tag{5}$$

After contracting the SU(2) indices and substituting the vevs

$$\begin{aligned}&\langle h_u^{(1)}\rangle=\langle h_d^{(2)}\rangle=0,\qquad \langle h_u^{(2)}\rangle=v_u,\qquad \langle h_d^{(1)}\rangle=v_d,\\ &\langle\varphi_T\rangle=(v_T,v_T,v_T),\qquad \langle\varphi_S\rangle=(v_S,0,0),\qquad \langle\xi\rangle=v_\xi,\end{aligned} \tag{6}$$

Eq. (5) reads

$$\begin{aligned}&\frac{1}{\sqrt{3}}L_2^{(1)}L_3^{(1)}v_uv_uv_S+\frac{1}{\sqrt{3}}L_1^{(1)}L_1^{(1)}v_uv_uv_\xi\\ &+\frac{1}{\sqrt{3}}L_2^{(1)}L_2^{(1)}v_uv_uv_\xi+\frac{1}{\sqrt{3}}L_3^{(1)}L_3^{(1)}v_uv_uv_\xi.\end{aligned} \tag{7}$$

Following these steps for all the terms in Eq. (3) yields the mass matrices for the charged leptons and the neutrinos:

$$M_{\ell^+} = \frac{v_d v_T}{M} \cdot \begin{array}{c} \\ L_1^{(2)} \\ L_2^{(2)} \\ L_3^{(2)} \end{array} \begin{array}{c} \begin{array}{ccc} e & \mu & \tau \end{array} \\ \begin{pmatrix} -\frac{1}{\sqrt{3}} & -\frac{1}{\sqrt{3}} & -\frac{1}{\sqrt{3}} \\ -\frac{1}{\sqrt{3}} & \frac{1}{2\sqrt{3}} & \frac{1}{2\sqrt{3}} \\ -\frac{1}{\sqrt{3}} & \frac{1}{2\sqrt{3}} & \frac{1}{2\sqrt{3}} \end{pmatrix} \end{array},$$

$$M_\nu = \frac{v_u v_u}{M^2} \cdot \begin{array}{c} \\ L_1^{(1)} \\ L_2^{(1)} \\ L_3^{(1)} \end{array} \begin{array}{c} \begin{array}{ccc} L_1^{(1)} & L_2^{(1)} & L_3^{(1)} \end{array} \\ \begin{pmatrix} \frac{v_\xi}{\sqrt{3}} & 0 & 0 \\ 0 & \frac{v_\xi}{\sqrt{3}} & \frac{v_S}{2\sqrt{3}} \\ 0 & \frac{v_S}{2\sqrt{3}} & \frac{v_\xi}{\sqrt{3}} \end{pmatrix} \end{array}. \tag{8}$$

Here, M denotes the cutoff scale of the theory, and suppresses the operators of mass dimension 5 and 6. In the case of Eq. (8), the bi-unitary transformations that diagonalize the charged lepton and neutrino mass matrices are independent of the Yukawa couplings, which we have therefore not indicated. The singular value decomposition (here in the special case where the number of rows is equal to the number of columns)

$$\hat{M}_{\ell^+} = D_L M_{\ell^+} D_R^\dagger, \qquad \hat{M}_\nu = U_L M_\nu U_R^\dagger \tag{9}$$

allows us to express the mass matrices as a product of a unitary matrix, a diagonal matrix with non-negative real numbers on the diagonal, and another unitary matrix where

$$D_{\mathrm{L}} = \begin{pmatrix} -0.5774 + i0.0000 & -0.5774 + i0.0000 & -0.5774 + i0.0000 \\ 0.5738 - i0.0636 & -0.2319 + i0.5287 & -0.3420 - i0.4652 \\ 0.5731 - i0.0702 & -0.3474 - i0.4612 & -0.2257 + i0.5314 \end{pmatrix},$$

$$U_{\mathrm{L}} = \begin{pmatrix} 0.0000 & -0.7071 & -0.7071 \\ -1.0000 & 0.0000 & 0.0000 \\ 0.0000 & 0.7071 & -0.7071 \end{pmatrix}. \tag{10}$$

The neutrino mixing matrix is, by definition,

$$U_{\mathrm{PMNS}} = D_{\mathrm{L}} U_{\mathrm{L}}^\dagger = \begin{pmatrix} 0.8165 + i0.0000 & 0.5774 + i0.0000 & 0.0000 + i0.0000 \\ 0.4058 - i0.0449 & -0.5738 + i0.0636 & 0.0778 + i0.7028 \\ 0.4052 - i0.0497 & -0.5731 + i0.0702 & -0.0860 - i0.7019 \end{pmatrix}. \tag{11}$$

To extract the mixing angles and phases, we use the explicit formulas presented in Ref. [28] and obtain

$$\theta_{12} = 35.26°, \qquad \theta_{23} = 45.00°, \qquad \theta_{13} = 0.00°, \tag{12}$$

which is tribimaximal mixing.

Several remarks are in order. In contrast to Ref. [16], where the matrices for the generators in the three-dimensional representation were wisely chosen so that M_{ℓ^+} is diagonal, our choice for the generators leads to a nondiagonal charged lepton mass matrix; see Eq. (8). We have checked that after changing to a basis where M_{ℓ^+} is diagonal (which corresponds to a redefinition of the charged lepton fields), our expressions for the Lagrangian, the mass matrices, and U_{PMNS} coincide with those in Ref. [16], and the same is true for the vevs. Our generators T_1, T_2, T_3 of A_4 are connected to those of Ref. [16] by $S \mapsto T_1 T_2^{-1} T_1$ and $T \mapsto T_2$.

We have written PYTHON programs that interact with GAP to get the generators, the character table, the dimensions of the conjugacy classes, and the explicit form of the matrices for all representations. From this, our code builds the Lagrangian that is invariant under all the symmetries, breaks the family symmetry, collects the terms that contribute to the charged lepton and neutrino mass matrices, and finally calculates the mixing matrix, the mixing angles, and the phases.

In Sec. IV, we present the results of our systematic scan for $A_4 \times C_3$, and finally in Sec. V, we discuss the results for all 76 flavor groups with special emphasis on the metacyclic groups T_7 and T_{13}.

IV. SYSTEMATIC SCAN OF $A_4 \times \mathbb{Z}_3$

We will now discuss the results that we obtained from the systematic scan of family symmetries, charge assignments, and vacuum configurations. We refer the reader also to Table III, where some of the results of this section are summarized.

It is important to stress that we are *not* specifically searching for tribimaximal mixing, but constructing *all models* for a given symmetry group (with the qualifications detailed in Sec. IV A).

We will only list inequivalent models: We consider two models to be equivalent, if their Lagrangians after contracting the family indices, but before symmetry breaking, are equal. In the plots, however, the data points correspond to vacua, and some may correspond to the *same* Lagrangian.

Since we will be discussing many different groups that may not all have a standard name, we will use their GAPIDs, and e.g. denote $A_4 \times C_3$ by $\mathfrak{G}(36, 11)$. The correspondence between the GAPIDs and the groups is given in Table III.

A. Particle content and family charge assignments

In Fig. 1 we show the flowchart of our systematic scan. The particles and their standard model charges are listed in the first two columns of Table II and will not be reproduced here. To avoid any misunderstandings, we emphasize that from now on ξ is on the same footing as φ_T and φ_S, and that its naming is simply a relic from earlier sections. The flavon fields may transform in any representation, and we scan over all possible vevs that have either 0 or 1 in each entry.

We restrict ourselves to such models where the lepton doublet L transforms in a three-dimensional representation, and e, μ, τ transform in one-dimensional representations of the family symmetry. Plausible as this may sound, there is no physics reason for that, but rather without these assumptions the number of family charge assignments quickly grows too large to allow for a systematic scan.

Regarding the Higgs sector, we will assume that there are exactly two fields. For one thing, we have supersymmetric models in mind that require an even number of Higgses. For another, more than two Higgs fields would spoil the unification of the gauge couplings. Thus, h_u, h_d are assigned any one-dimensional representation.

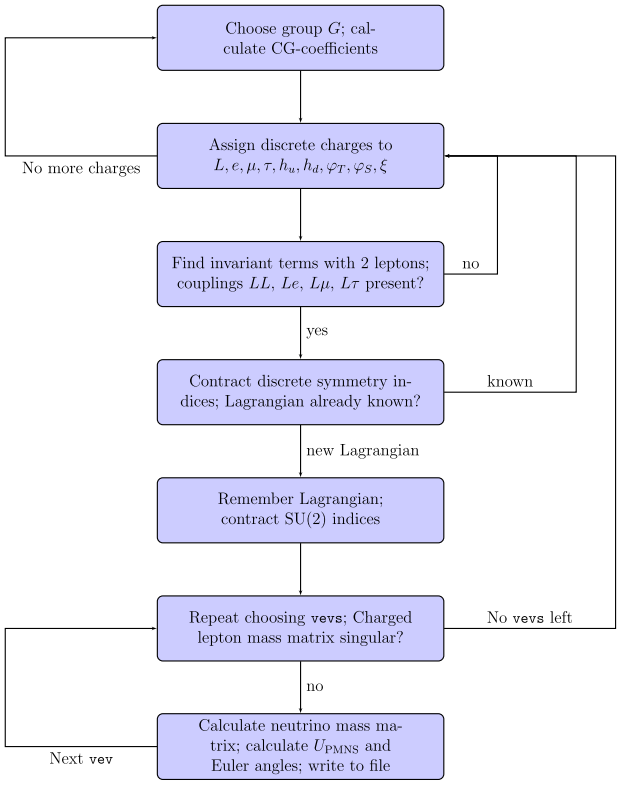

FIG. 1 (color online). Systematic scan for models with family symmetry G and up to three flavon fields.

B. Models for $A_4 \times \mathbb{Z}_3$

We will start with the results for the "classic" group $\mathfrak{G}(36, 11) = A_4 \times C_3$. The 14 594 580 family charge assignments to L, e, μ, τ, h_u, h_d, φ_T, φ_S, ξ give 39 900 inequivalent Lagrangians out of which 22 932 have non-singular charged lepton and neutrino mass matrices.

In this set, we find 4233 models of tribimaximal mixing (18.5%). For a given model, there may exist more than one vacuum configuration that leads to TBM (e.g. six vevs for the model in Sec. III), and we have *not* counted them separately. In the 3σ range there are 4481 models (19.5%). We find no models that lie in the 1σ range, because $\theta_{13} = 0°$ is excluded at 1σ (cf. Table I). This fact is nicely illustrated in the third plot of Fig. 2(b): The 1σ range, represented by the green band, is empty.

Figure 2 shows the distribution of the mixing angles θ_{12}, θ_{23}, and θ_{13}, where we are now counting the *vacua* and not the models. The reason for this is that for one and the same Lagrangian, the values of the mixing angles will, in general, depend on the choice of vacuum. The histograms in Fig. 2(a) have 15 992 118 entries, reflecting the fact that for each of the 39 900 inequivalent Lagrangians, we are looping over 8 to 512 vacua, depending on the dimensions of the irreducible representations (irreps) assigned to the flavon fields.

The area of each histogram has been normalized to 1 and the bin width is 1°, so the y axis gives the *percentage* of vacua that produce the angles on the x axis. The green and yellow bands correspond to the 1σ and 3σ ranges, respectively (cf. Table I). In Fig. 2(a), we simply count the number of times that a given angle is reproduced, irrespective of the values that the two other angles may take. For example, from the first histogram we can read off that 7.6% of the vacua give a value for θ_{12} that is consistent with experiment at 3σ, where θ_{23} and θ_{13} can take any values.

Now we investigate whether we can obtain some predictions by introducing priors. In Fig. 2(b) we have restricted two of the angles to their 3σ intervals and plotted the third one. As a consequence, the numbers of entries in the histograms are not equal.

The most striking difference between Figs. 2(a) and 2(b) is that now the most likely value for θ_{23} is 45° and it lies in the 1σ interval. Furthermore, the number of vacua in the experimentally disfavored region has decreased significantly, and 58% of the vacua are in the 3σ interval.

For θ_{13}, values near 90° are now excluded, and the 3σ interval is almost depopulated except for $\theta_{13} = 0°$ and some very few models with $\theta_{13} \neq 0°$. Since $\theta_{13} = 0°$ is now by far the most likely value, this can be interpreted as a strong hint for θ_{13} to be 0° (at leading order) based on current experimental data and the theoretical assumption of

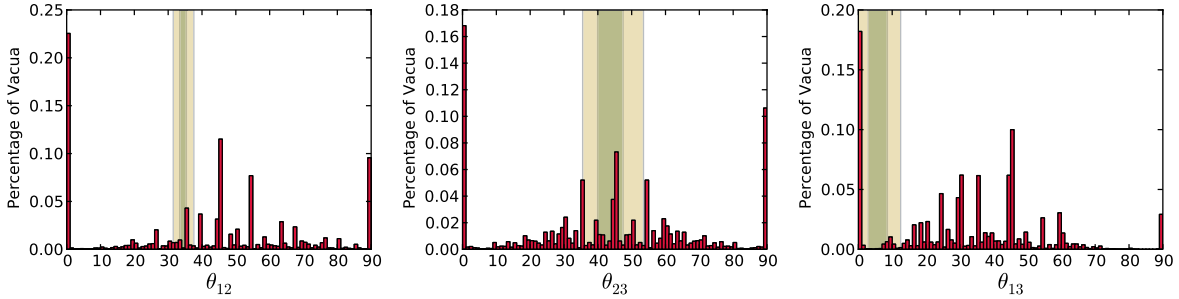

(a) Number of vacua that give θ_{ij} with no constraints on the other 2 angles. Each histogram has 15992118 entries.

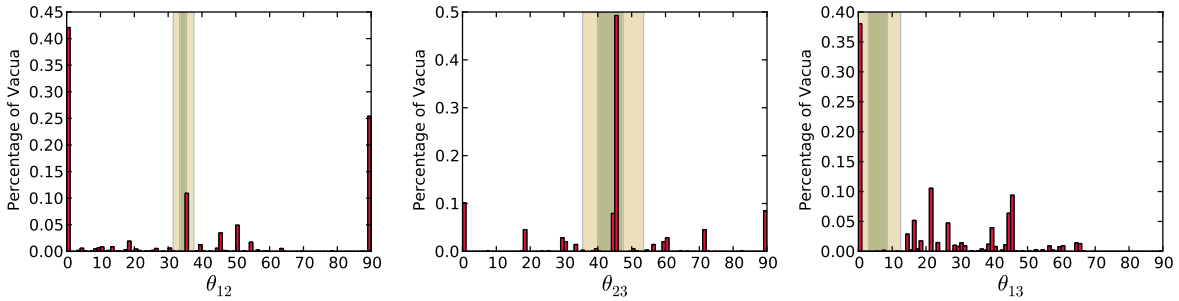

(b) Number of vacua that give θ_{ij} with the other 2 angles restricted to their 3σ interval. The histograms have 838289, 148886 and 225844 entries, respectively.

FIG. 2 (color online). Number of vacua with family symmetry $\mathfrak{G}(36, 11) = A_4 \times C_3$ that give the mixing angles denoted on the x axis. The area of the histograms is normalized to 1 and the bin width is 1. The green and yellow (dark and light gray) bands correspond to the 1σ and 3σ ranges, respectively.

an $A_4 \times \mathbb{Z}_3$ family symmetry. We find that 38% of the vacua are in the 3σ interval.

For θ_{12}, the most likely value is still 0°, but 35° is now the third most likely angle. Clearly, the experimental data on θ_{23} and θ_{13} are pushing us in the right direction. 11% of the vacua are in the 3σ interval.

It is an interesting observation that the effect of our restricting two out of three angles to their 3σ interval was such that the preference of the data for the experimentally allowed ranges became much more pronounced. This is an unexpected and nontrivial result and may further testify to the phenomenological viability of A_4.

To learn more about the correlation of the angles and how priors may affect them, in Fig. 3 we present the distribution of two out of three angles, respectively. The color bar on the right-hand side of each figure gives the correspondence between the colors in the plots and the logarithm to base 10 of the number of vacua with the angles θ_{ij} and θ_{mn} on the x and y axes, respectively.

In Fig. 3(a), each two-dimensional histogram has 15 992 118 entries which correspond to the full set of vacua that we had also previously considered in Fig. 2(a). In analogy to Fig. 2(a), we have imposed no constraints on the third angle which is not plotted. From the first plot, we cannot read off much, except that there exist certain ''hot spots'' (e.g. $\theta_{12} = 0°$ and $\theta_{23} = 45°$) that correspond to large numbers of vacua, and that the regions near the lower corners are, by comparison, less populated. In the second and third plots, we see that there are considerably fewer models for $\theta_{12} \gtrsim 70°$ and $\theta_{23} \gtrsim 75°$, respectively. In the case of the second plot, this holds even for much lower values of $\theta_{12} \gtrsim 35°$, given that θ_{13} is not larger than $\sim 15°$ or near 0°.

In Fig. 3(b), we present the same correlations as in Fig. 3(a), but this time, we have required that the third angle be in its 3σ interval. As a consequence, the numbers of entries in the histograms are not equal. We have used the same normalization of the color bars in Figs. 3(a) and 3(b) to facilitate comparisons between them.

Considering the first plot, we can see that most vacua lie in a band $\theta_{12} \simeq 30°$–$60°$, whereas this effect becomes less pronounced for $\theta_{23} \simeq 15°$–$30°$. For $\theta_{23} \simeq 45°$, values of $\theta_{12} = 0°, 35°, 55°, 90°$ are favored (red bins in plot).

The second plot clearly shows that $\theta_{12} \gtrsim 70°$ and, to a lesser extent, $\theta_{12} \lesssim 10°$ are disfavored. For $\theta_{12} \simeq 10°$–$70°$, a band of $\theta_{13} = 0°$–$10°$ that widens with increasing θ_{12} is sparsely populated, but note that for $\theta_{13} = 0°$ and $\theta_{12} = 45°$, there is one of the highest counts of vacua in the plot as indicated by the red bins. This is consistent with our previous observation from Fig. 2(b) that $\theta_{13} = 0°$ is preferred, but that otherwise the region $\theta_{13} \lesssim 10°$ is disfavored.

In the third plot we again observe a band structure $\theta_{23} \simeq 15°$–$60°$ where most of the vacua are concentrated, and find that $\theta_{13} \lesssim 10°$ and $\theta_{13} \gtrsim 80°$ are disfavored. The combination $\theta_{23} \simeq 45°$ and $\theta_{13} = 0°$, however, is

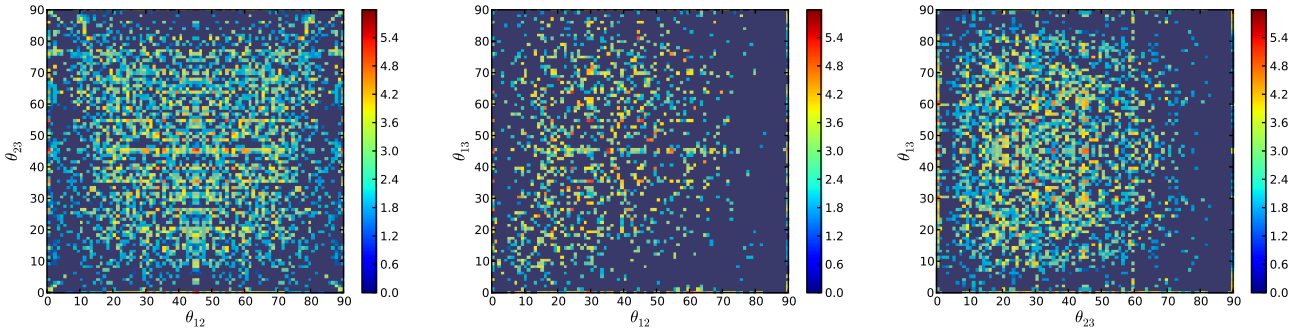

(a) Number of vacua that give θ_{ij} and θ_{mn} with no constraint on the remaining angle. Each histogram has 15992118 entries.

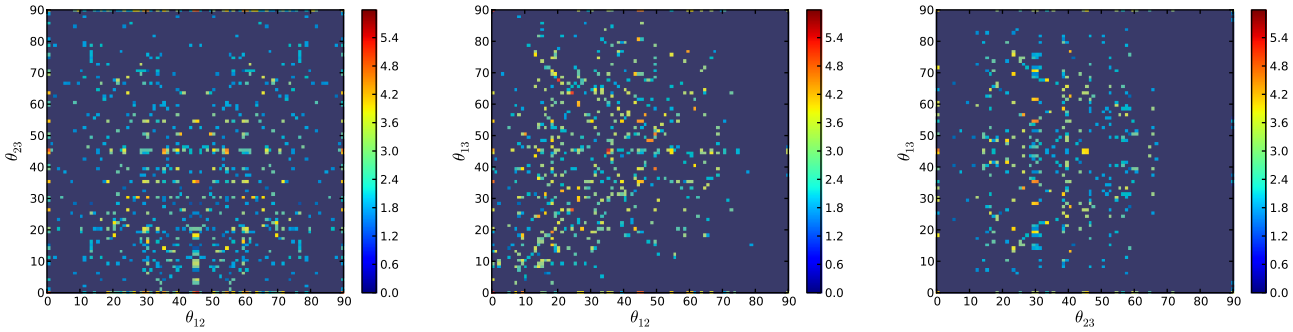

(b) Number of vacua that give θ_{ij} and θ_{mn} with the remaining angle restricted to its 3σ interval. The histograms have 2941000, 3675600 and 1057170 entries, respectively.

FIG. 3 (color online). Logarithmic plot of the number of vacua with family symmetry $\mathfrak{G}(36, 11) = A_4 \times C_3$ that give the mixing angles denoted on the axes. The bin width on both axes is 1. The base of the logarithm is 10, and the color map on the right side of each plot gives the exponents.

not preferred. As indicated by the red bins, the most likely combination of angles lies elsewhere.

Ideally, to give a graphical representation of the full information on the angles and their correlations, we would create a three-dimensional histogram with θ_{12}, θ_{23}, and θ_{13} on the axes, and plot the number of vacua along a fourth dimension. Since this is not feasible, we present a plot in three dimensions, where the color of the data points indicates the number of vacua.

In Fig. 4(a), each point represents a bin in a three-dimensional histogram: If there is at least one vacuum that produces the angles $(\theta_{12}, \theta_{23}, \theta_{13})$, we set a point at the respective coordinates. The bin width on each axis is 1, and in total there are $90 \times 90 \times 90$ bins, of which 5528 are not empty. The color of the point denotes the logarithm to base 10 of the number of vacua that give the respective angles, where the colors from blue to red (dark to light gray) correspond to an increasing number of vacua. We have not displayed the color map for the plots, since we find it difficult to extract quantitative information from the three-dimensional representation and rather use it as a means of uncovering correlations between the angles and the qualitative features of A_4 as a symmetry group.

In Fig. 4(b), we display only those 1287 bins that have more than 1000 entries. This removes much of the clutter-ing and gives a clearer picture regarding where the most likely vacua are concentrated. One immediate observation is that the parameter space for $(\theta_{12}, \theta_{23}, \theta_{13})$ is not uniformly populated: There are very few vacua for $\theta_{12} \simeq 60°$–$90°$; low and high values of θ_{13} are disfavored (except $\theta_{13} = 0°$); and rotating Fig. 4(b) to view it from different perspectives, we see that most of the vacua are concentrated in a volume $\theta_{12} \simeq 10°$–$60°$, $\theta_{23} \simeq 20°$–$70°$, $\theta_{13} \gtrsim 15°$.

Considering the θ_{12}–θ_{23} plane of Fig. 4(b) that corresponds to $\theta_{13} = 0°$, we find that $\theta_{12} = \theta_{23} = 45°$ are the most likely values (see red points), which is in agreement with the first plot in Fig. 3(a).

Regrettably, we fail to see any preference for tribimaximal mixing or the experimentally allowed values. Without putting in at least some priors, the best we can do is set approximate upper and lower bounds on the angles.

It is also worth mentioning that TBM can be realized with the smaller flavor group $\mathfrak{G}(24, 13) = A_4 \times C_2$, where the C_3 factor of the model in Ref. [16] has been replaced by a C_2. As we will see from Fig. 5 in Sec. VA, it is the second smallest discrete group for which we find TBM.

C. A model with $\theta_{13} \simeq 5°$

Recently some analyses have reported on possible hints of a nonzero θ_{13} [6,17,18]. A model with $0° \lneqq \theta_{13} \leq 8.6°$

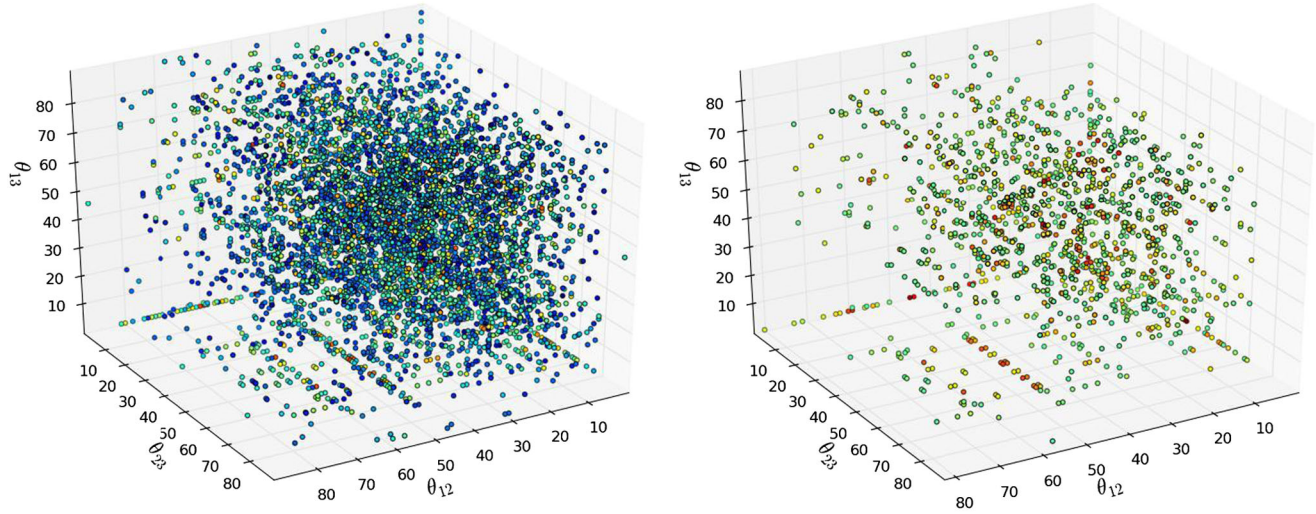

(a) The 5,528 bins that are ≥ 1. (b) The 1,287 bins that are ≥ 1000.

FIG. 4 (color online). Number of vacua that give θ_{12}, θ_{23}, θ_{13}. Each point corresponds to a bin in the three-dimensional histogram that has at least one entry. The bin width is 1. The color of the points (from blue to red/dark to light gray) corresponds to the logarithm to base 10 of the number of vacua (from lower to higher). The color map is the same as in Fig. 3.

that lies in the 1σ interval is easily constructed. For the family symmetry, we take $\mathfrak{G}(36, 11) = A_4 \times C_3$ and assign the family charges $(L, e, \mu, \tau, h_u, h_d, \varphi_T, \varphi_S, \xi) \sim (\mathbf{3}, \mathbf{1}, \mathbf{1^{(4)}}, \mathbf{1'''}, \mathbf{1'}, \mathbf{1^{(7)}}, \mathbf{1^{(5)}}, \mathbf{3''}, \mathbf{3''})$. When the flavon fields acquire vevs along the directions $\langle\varphi_T\rangle = (1)$, $\langle\varphi_S\rangle = (1, 0, 1)$, $\langle\xi\rangle = (1, 1, 1)$, we obtain the mixing angles $\theta_{12} = 33.9°$, $\theta_{23} = 40.9°$, and $\theta_{13} = 5.1°$ that all lie in the 1σ interval of the experimentally determined values. Incidentally, we have chosen the model in such a way as to produce a θ_{13} that is close to the present best-fit value of Ref. [6] with the modified Gallium cross section.

V. RESULTS FOR 76 FLAVOR GROUPS

In the list of all groups of order ≤ 100 [24], we find 90 groups which have a three-dimensional representation (see Table III). For 14 groups, a systematic scan would take more than 60 days. In this section, we present the results for those 76 groups that can be analyzed in a reasonable time.

A. Tribimaximal and experimentally allowed models

One main result of our analysis is that we have found thousands of new models that give exact tribimaximal mixing. Figure 5 shows the number of inequivalent models (not vacua) for the 76 groups specified before. The red bars indicate the fraction of Lagrangians for which at least one choice of vevs leads to tribimaximal mixing, and the green bars give the number of models that lie in the 3σ interval of the measured angles. The correspondence between the GAPIDs on the x axis and the full name of the group is given in Table III, where we also list the exact numbers of models that may be difficult to read off from the graph.

The conspicuous gaps in Fig. 5 are a consequence of our criterion that the mass matrices be nonsingular; i.e. we do not consider such cases where any of the neutrinos (or charged leptons) are massless.

Out of the 76 groups that we scanned, nine (12%) have only singular mass matrices. We see that 44 groups (58%)

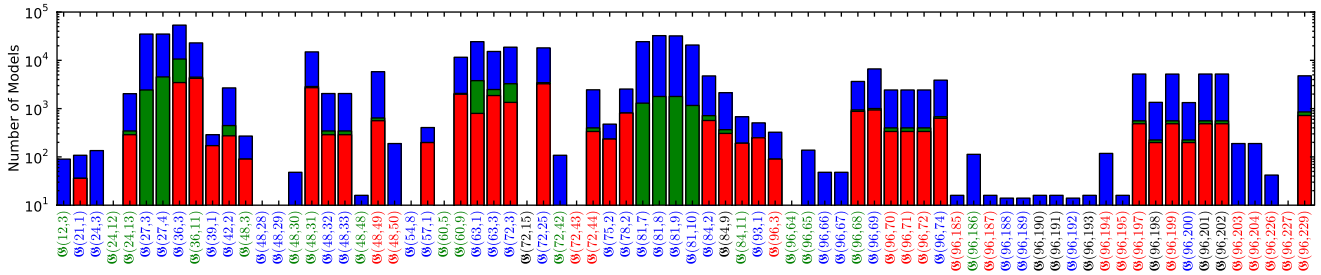

FIG. 5 (color online). The number of models per symmetry group. On the x axis, we label the flavor symmetry $\mathfrak{g}$ by its GAPID, cf. Table III. The red and blue labels on the x axis indicate that $\mathfrak{g} \supset A_4$ and $\mathfrak{g} \subset \mathrm{U}(3)$, respectively, whereas green signifies that both conditions are satisfied simultaneously. Along the y axis, the blue bars give the number of Lagrangians that lead to *nonsingular* mass matrices. The green bars indicates the number of models that lie within the 3σ interval, and the red bars finally give the number of models for which at least one vacuum configuration gives tribimaximal mixing. If the colors are not visible, please refer to Table III which contains the same information.

lie in the 3σ interval, and 38 (50%) are even tribimaximal (for at least one vacuum configuration, respectively). Only for 23 groups (30%) we could not find any vacuum configuration that satisfies the experimental limits. Note, though, that despite being very general, our scan is not fully comprehensive, since (i) we assume that the lepton doublet transforms in a triplet, and (ii) we do not scan over all possible vevs. Owing to this fact, there may exist even more viable models than we have identified.

The smallest group for which we find TBM is $\mathfrak{G}(21, 1) = T_7$. Note that we do not have any additional Abelian factors $\mathbb{Z}_n$, as is the case with many A_4 models in the literature. In this sense, we have identified T_7 as the minimal flavor symmetry that can produce TBM. Incidentally, T_7 is the smallest group after A_4 that has a three-dimensional irreducible representation. We will take a closer look at T_7 in Sec. V B.

An interesting observation from Fig. 5 is that for nine groups the models with TBM are identical to those that are consistent with experiment at 3σ; i.e. the green bars are completely covered by the red ones: $\mathfrak{G}(21, 1) = T_7$, $\mathfrak{G}(39, 1) = T_{13}$, $\mathfrak{G}(48, 3) = \Delta(48)$, $\mathfrak{G}(57, 1) = T_{19}$, $\mathfrak{G}(75, 2) = \Delta(75)$, $\mathfrak{G}(78, 2) = T_{26}$, $\mathfrak{G}(84, 11)$, $\mathfrak{G}(93, 1) = T_{31}$, and $\mathfrak{G}(96, 3)$ (see also Table III). Five of these nine groups belong to the T series of SU(3) subgroups [30].

B. The flavor group T_7

As mentioned before, T_7 [31–33] is the smallest group for which we find tribimaximal mixing.

In Fig. 6 we show for $\mathfrak{G}(21, 1) = T_7$ the distribution of the mixing angles. If we use the experimental data on two of the angles and plot the multiplicity of the third one, we find that $\theta_{12} \simeq 35^\circ$ is the second-most likely angle to be produced, and the only one within the 3σ interval. For θ_{23}, we obtain a unique prediction $\theta_{23} = 45^\circ$. As for θ_{13}, the value 0° is both the most likely angle and the only one attained within the 3σ interval.

Remarkably, the 3σ bands in Fig. 6(b) are completely depopulated except for the values corresponding to exact tribimaximal mixing. In this sense one can say that in light of the experimental data, assuming a T_7 family symmetry predicts TBM.

As one can see from Table III, for T_7 the number of experimentally allowed models coincides with the number of tribimaximal ones. This is a slightly weaker statement than the one made in the previous paragraph, since we list a model as TBM or experimentally allowed, if there exists at least one vacuum configuration for which this is true. These vacua need not be the same, and there may exist others for which the model is neither allowed nor TBM. In contrast, Fig. 6(b) shows that, independently of the choice

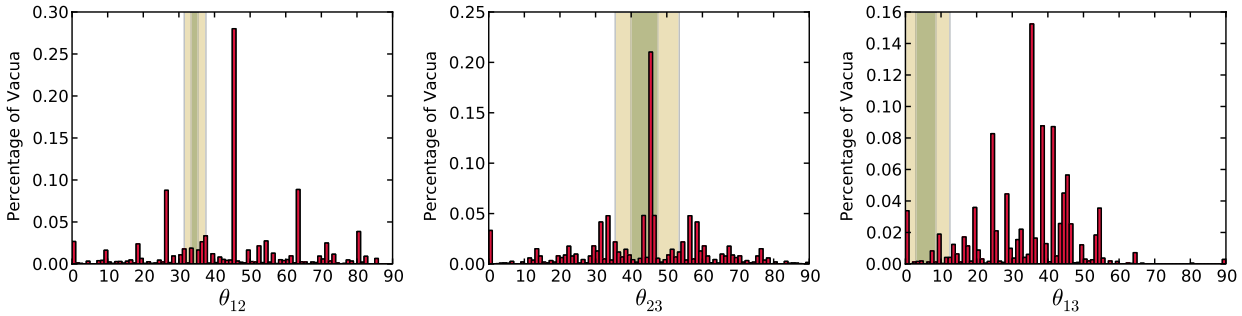

(a) Number of vacua that give θ_{ij} with no constraints on the other 2 angles.

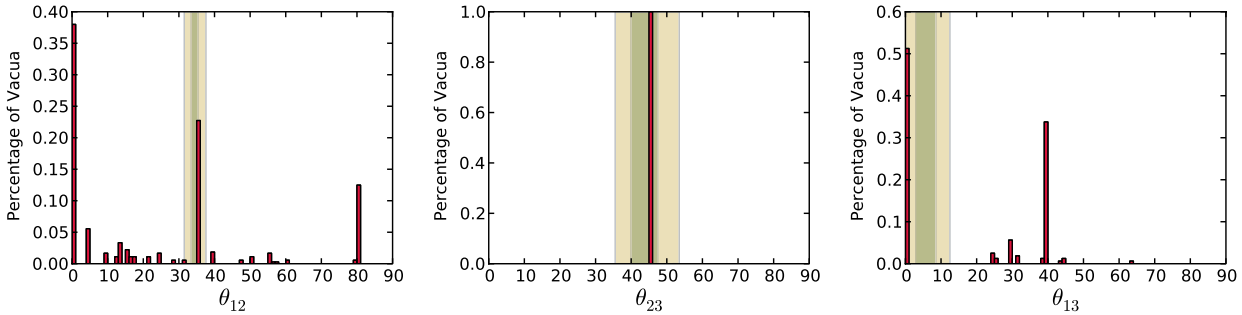

(b) Number of vacua that give θ_{ij} with the other 2 angles restricted to their 3σ interval.

FIG. 6 (color online). Number of vacua with family symmetry $\mathfrak{G}(21, 1) = T_7$ that give the mixing angles denoted on the x axis. The area of the histograms is normalized to 1 and the bin width is 1. The green and yellow bands correspond to the 1σ and 3σ ranges, respectively.

of vacuum, requiring the mixing angles to be in the 3σ bands automatically leads to tribimaximal mixing.

The other plots relating to T_7 can be found in Sec. 2 of Ref. [34].

C. The flavor group T_{13}

Let us now turn our attention to $\mathfrak{G}(39, 1) = T_{13}$. One reason why this group stands out is that 59% of its models are tribimaximal (see Table III). As compared to e.g. $A_4 \times C_3$ with 18.5%, this is a much larger fraction.

Again, as was the case for T_7, any model that has a vacuum for which the mixing angles are consistent with experiment at the 3σ level also allows for TBM to be realized (see Table III).

From Fig. 7(b) we see that the correlation between the family symmetry T_{13} and tribimaximal mixing is almost as strong as in the case of T_7. Contrary to the case of T_7, not every vacuum that is consistent with experiment leads to TBM; i.e. we can find some vacua in the 3σ band that are not tribimaximal, but this is mainly a consequence of the large errors on θ_{13}. Remarkably, all three histograms in Fig. 7(b) peak at values corresponding to tribimaximal mixing.

The other plots relating to T_{13} can be found in Sec. 9 of Ref. [34].

D. The other flavor groups

In Ref. [34] we present the graphs (analogous to those in Sec. IV) for all 67 flavor groups that have nonsingular mass matrices (cf. Sec. VA). Since a detailed discussion of the results for all groups is beyond the scope of the present publication, we will limit ourselves to some qualitative observations.

From the discussion in the previous sections, one may get the impression that realizing TBM is not too difficult as long as one scans over a large enough fraction of the parameter space. Figure 1(b) of Ref. [34] for $\mathfrak{G}(12, 3) = A_4$, however, shows that there are groups for which the experimentally determined mixing angles cannot be reproduced within their 3σ error bands. Other examples with a larger flavor group are [34] $\mathfrak{G}(48, 30)$ or $\mathfrak{G}(96, 65)$. Of course, this statement depends on the assumptions that we used to constrain the Lagrangian, e.g. the number of flavon fields.

T_{13} is, by far, not the only group with the remarkable property that restricting two of the angles to their respective 3σ intervals predicts the third one in the sense that it is the most likely value. Other examples are [34] $\mathfrak{G}(57, 1) = T_{19}$, $\mathfrak{G}(75, 2) = \Delta(75)$, and $\mathfrak{G}(93, 1) = T_{31}$.

In analogy to T_7 there exist other groups for which restricting all three angles to their respective 3σ intervals

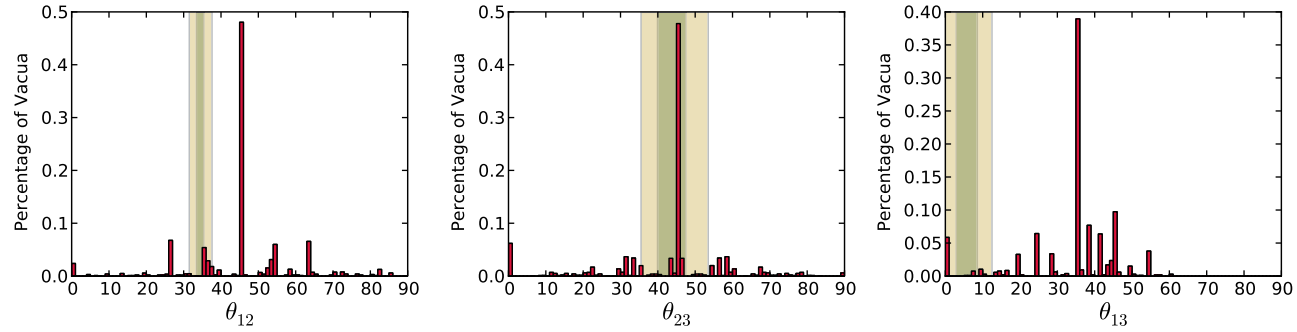

(a) Number of vacua that give θ_{ij} with no constraints on the other 2 angles.

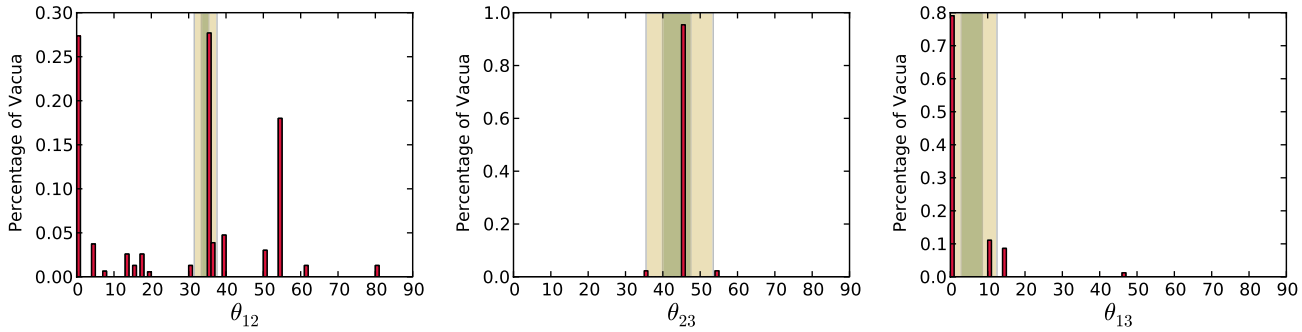

(b) Number of vacua that give θ_{ij} with the other 2 angles restricted to their 3σ interval.

FIG. 7 (color online). Number of vacua with family symmetry $\mathfrak{G}(39, 1) = T_{13}$ that give the mixing angles denoted on the x axis. The area of the histograms is normalized to 1 and the bin width is 1. The green and yellow bands correspond to the 1σ and 3σ ranges, respectively.

almost always leads to TBM, e.g. $\mathfrak{G}(48, 31)$, $\mathfrak{G}(60, 9)$, $\mathfrak{G}(72, 25)$. In contrast to T_7, however, there are a few vacua in the 3σ interval that do not realize TBM.

From Fig. 21(a) of Ref. [34], for $\mathfrak{G}(36, 3)$ we see that there exist groups that predict a uniform distribution of the mixing angles so that, in comparison, the distribution for $A_4 \times C_3$ (see Fig. 4) clearly shows some preference for certain regions of the parameter space.

E. Is there a connection between A_4 and tribimaximal mixing?

To explore the connection between tribimaximal mixing and A_4, we have color coded the group names on the x axis of Fig. 5. Blue, red, and green bars correspond to $\mathfrak{g} \subset \mathrm{U}(3)$, $\mathfrak{g} \supset A_4$, and $A_4 \subset \mathfrak{g} \subset \mathrm{U}(3)$, respectively. The same information is summarized in Table III. Of the 76 groups, 35 contain A_4 as a subgroup, but only for 16 out of these 35 groups we can find vacua that give models of tribimaximal mixing. It is conceivable, though, that one may find TBM models for the other groups, if one introduces more than three flavon fields.

We find four groups, $\mathfrak{G}(84, 9)$, $\mathfrak{G}(96, 198)$, $\mathfrak{G}(96, 201)$, and $\mathfrak{G}(96, 202)$, that are not subsets of U(3) nor do they contain an A_4 subgroup; nevertheless, they can accommodate models of tribimaximal mixing.

In light of these facts, it is difficult to maintain that A_4 is special with regard to realizing tribimaximal mixing. We strongly advocate not neglecting other promising groups, especially T_7 and T_{13}.

VI. CONCLUSIONS

In this publication we scanned 76 groups and constructed a total of 439 820 Lagrangians, out of which 59 019 were consistent with experiment and 31 137 were tribimaximal. The large set of viable models allowed us to look at correlations between the mixing angles and make a prediction for θ_{13} that will be measured in upcoming experiments.

We have presented an explicit model with $\theta_{13} = 5.1^\circ$ to show that the recent tentative hints of a nonzero θ_{13} can be accommodated. We found tribimaximal mixing in 38 flavor groups; most of these groups had not been considered for model building before. We hope that the calculational tools and methods that we have outlined will be useful for future model building efforts.

We would like to emphasize that we do not advocate a probabilistic approach to model building along the lines of the landscape idea in string theory. Rather, we are trying to maximize our chances of finding the correct model(s) by starting out with a large set that reproduces the mixing angles within the current experimental limits. In the future, we plan to take this analysis several steps further and look at the generation of mass hierarchies and the vacuum alignment problem, and finally include the quark sector. Invariably, each step will drastically reduce the number of models, and the goal is to find at least one that passes all criteria.

On the other hand, for answering the question as to whether any discrete flavor group is inherently connected to tribimaximal mixing, a probabilistic approach may be useful: The easier tribimaximal mixing can be realized in a given group, the more pronounced the connection is. In this sense, A_4 fares well, but T_7 and T_{13} should be considered to be on equal footing, if not more promising.

ACKNOWLEDGMENTS

We acknowledge useful discussions with Christoph Luhn, Stuart Raby, and Sudhir Vempati. A. W. would like to thank Jörg Meyer for drawing his attention to PYTHON and PYROOT, and for always patiently answering his ROOT questions. We would like to thank the GAP Forum and, in particular, Vahid Dabbaghian, Alexander Hulpke, and Martin Schönert for their support. A. W. would like to thank the Korean Institute for Advanced Study and Eung-Jin Chun for their hospitality during the final stages of this work. K. P. would like to thank the Indian Institute of Science and Sudhir Vempati, and acknowledges support from the Department of Science and Technology of the Government of India under the grant "Complementarity from Direct and Indirect Searches of Supersymmetry." We are greatly indebted to the Centre de Calcul de l'Institut National de Physique Nucléaire et Physique des Particules for allowing us to use their resources. We thank Geneviève Bélanger, Gautam Bhattacharyya, J. F. Cornwell, Amol Dighe, Sabine Kraml, Patrick Otto Ludl, Jong-Chul Park, and Tzvetalina Stavreva for comments and suggestions.

APPENDIX A: LIST OF GROUPS OF ORDER AT MOST 100

Very few groups have been given dedicated names by the mathematicians and physicists who studied them. Examples are the cyclic groups C_n, the symmetric groups S_n, the alternating groups A_n, and the dihedral groups D_n. The vast majority are described by their substructure and a "prescription" of how to put these parts together to form the full group: the direct product, the semidirect product, and the short exact sequence. The reader who is unfamiliar with any of these concepts may refer to e.g. Ref. [35].

Since the list of 1048 groups of order ≤ 100 is too long to include in the present publication, we have made it available for download [24]. For details on the generation of this list, see Appendix B.

The list of the 90 groups of order ≤ 100 that have a three-dimensional irreducible representation and that we have systematically scanned for viable models of lepton flavor is given in Table III.

TABLE III. The 90 groups of order ≤ 100 that have a three-dimensional irreducible representation. For details, refer to Appendix A 2.

GAPID	Group	U_3	U_2	$U_{2\times1}$	A_4	Models	3σ	TBM
[12, 3]	A_4	✓✓	×	×	✓	90	0	0
[21, 1]	$C_7 \rtimes_\varphi C_3$	✓✓	×	×	×	108	36	36
[24, 3]	SL(2, 3)	✓✓	✓✓	✓✓	×	135	0	0
[24, 12]	S_4	✓✓	×	×	✓	0	0	0
[24, 13]	$C_2 \times A_4$	✓	×	×	✓	2034	344	288
[27, 3]	$(C_3 \times C_3) \rtimes_\varphi C_3$	✓✓	×	×	×	34 992	2430	0
[27, 4]	$C_9 \rtimes_\varphi C_3$	✓	×	×	×	34 992	4536	0
[36, 3]	$(C_2 \times C_2) \rtimes_\varphi C_9$	✓	×	×	×	53 535	10 621	3459
[36, 11]	$C_3 \times A_4$	✓✓	×	×	✓	22 932	4481	4233
[39, 1]	$C_{13} \rtimes_\varphi C_3$	✓✓	×	×	×	288	171	171
[42, 2]	$C_2 \times (C_7 \rtimes_\varphi C_3)$	✓	×	×	×	2682	445	273
[48, 3]	$(C_4 \times C_4) \rtimes_\varphi C_3$	✓✓	×	×	✓	270	90	90
[48, 28]	$\mathrm{SL}(2, 3) \rightarrow G \rightarrow C_2$	✓✓	✓✓	✓✓	×	0	0	0
[48, 29]	GL(2, 3)	✓✓	✓	✓	×	0	0	0
[48, 30]	$A_4 \rtimes_\varphi C_4$	✓	×	×	✓	48	0	0
[48, 31]	$C_4 \times A_4$	✓	×	×	✓	14 937	2864	2712
[48, 32]	$C_2 \times \mathrm{SL}(2, 3)$	✓	×	✓✓	×	2052	344	288
[48, 33]	$\mathrm{SL}(2, 3) \rtimes_\varphi C_2$	✓✓	✓	✓	×	2052	344	288
[48, 48]	$C_2 \times S_4$	✓	×	×	✓	16	0	0
[48, 49]	$C_2 \times C_2 \times A_4$	×	×	×	✓	5805	640	561
[48, 50]	$(C_2 \times C_2 \times C_2 \times C_2) \rtimes_\varphi C_3$	×	×	×	✓	189	0	0
[54, 8]	$((C_3 \times C_3) \rtimes_\varphi C_3) \rtimes_\varphi C_2$	✓✓	×	×	×	0	0	0
[54, 10]	$C_2 \times ((C_3 \times C_3) \rtimes_\varphi C_3)$	✓	×	×	×	—	—	—
[54, 11]	$C_2 \times (C_9 \rtimes_\varphi C_3)$	✓	×	×	×	—	—	—
[57, 1]	$C_{19} \rtimes_\varphi C_3$	✓✓	×	×	×	405	198	198
[60, 5]	A_5	✓✓	×	×	✓	0	0	0
[60, 9]	$C_5 \times A_4$	✓	×	×	✓	11 575	2063	1983
[63, 1]	$C_7 \rtimes_\varphi C_9$	✓	×	×	×	24345	3792	795
[63, 3]	$C_3 \times (C_7 \rtimes_\varphi C_3)$	✓✓	×	×	×	15 246	2483	1863
[72, 3]	$Q_8 \rtimes_\varphi C_9$	✓✓	✓	✓✓	×	18 714	3272	1344
[72, 15]	$((C_2 \times C_2) \rtimes_\varphi C_9) \rtimes_\varphi C_2$	×	×	×	×	0	0	0
[72, 16]	$C_2 \times ((C_2 \times C_2) \rtimes_\varphi C_9)$	✓	×	×	×	—	—	—
[72, 25]	$C_3 \times \mathrm{SL}(2, 3)$	✓✓	✓	✓✓	×	18 105	3441	3261
[72, 42]	$C_3 \times S_4$	✓✓	×	×	✓	108	0	0
[72, 43]	$(C_3 \times A_4) \rtimes_\varphi C_2$	×	×	×	✓	0	0	0
[72, 44]	$A_4 \times S_3$	×	×	×	✓	2451	399	336
[72, 47]	$C_6 \times A_4$	✓	×	×	✓	—	—	—
[75, 2]	$(C_5 \times C_5) \rtimes_\varphi C_3$	✓✓	×	×	×	477	234	234
[78, 2]	$C_2 \times (C_{13} \rtimes_\varphi C_3)$	✓	×	×	×	2541	810	810
[81, 3]	$(C_9 \times C_3) \rtimes_\varphi C_3$	×	×	×	×	—	—	—
[81, 4]	$C_9 \rtimes_\varphi C_9$	×	×	×	×	—	—	—
[81, 6]	$C_{27} \rtimes_\varphi C_3$	✓	×	×	×	—	—	—
[81, 7]	$(C_3 \times C_3 \times C_3) \rtimes_\varphi C_3$	✓	×	×	×	24 329	1296	0
[81, 8]	$(C_9 \times C_3) \rtimes_\varphi C_3$	✓	×	×	×	32 416	1782	0
[81, 9]	$(C_9 \times C_3) \rtimes_\varphi C_3$	✓✓	×	×	×	32 076	1782	0
[81, 10]	$(C_3 \times C_3) \rightarrow G \rightarrow (C_3 \times C_3)$	✓	×	×	×	20 736	1161	0
[81, 12]	$C_3 \times ((C_3 \times C_3) \rtimes_\varphi C_3)$	×	×	×	×	—	—	—
[81, 13]	$C_3 \times (C_9 \rtimes_\varphi C_3)$	×	×	×	×	—	—	—
[81, 14]	$(C_9 \times C_3) \rtimes_\varphi C_3$	✓	×	×	×	—	—	—
[84, 2]	$C_4 \times (C_7 \rtimes_\varphi C_3)$	✓	×	×	×	4752	714	567
[84, 9]	$C_2 \times C_2 \times (C_7 \rtimes_\varphi C_3)$	×	×	×	×	2136	366	306
[84, 10]	$C_7 \times A_4$	✓	×	×	✓	—	—	—

TABLE III. (*Continued*)

GAPID	Group	U_3	U_2	$U_{2\times1}$	A_4	Models	3σ	TBM
[84, 11]	$(C_{14} \times C_2) \rtimes_\varphi C_3$	✓✓	×	×	✓	678	192	192
[93, 1]	$C_{31} \rtimes_\varphi C_3$	✓✓	×	×	×	507	249	249
[96, 3]	$((C_4 \times C_2) \rtimes_\varphi C_4) \rtimes_\varphi C_3$	×	×	×	✓	324	90	90
[96, 64]	$((C_4 \times C_4) \rtimes_\varphi C_3) \rtimes_\varphi C_2$	✓✓	×	×	✓	0	0	0
[96, 65]	$A_4 \rtimes_\varphi C_8$	✓	×	×	✓	138	0	0
[96, 66]	$\mathrm{SL}(2,3) \rtimes_\varphi C_4$	✓	×	✓✓	×	48	0	0
[96, 67]	$\mathrm{SL}(2,3) \rtimes_\varphi C_4$	✓✓	✓	✓	×	48	0	0
[96, 68]	$C_2 \times ((C_4 \times C_4) \rtimes_\varphi C_3)$	✓	×	×	✓	3648	939	876
[96, 69]	$C_4 \times \mathrm{SL}(2,3)$	✓	×	✓✓	×	6637	1002	936
[96, 70]	$((C_2 \times C_2 \times C_2 \times C_2) \rtimes_\varphi C_3) \rtimes_\varphi C_2$	×	×	×	✓	2433	399	336
[96, 71]	$((C_4 \times C_4) \rtimes_\varphi C_3) \rtimes_\varphi C_2$	×	×	×	✓	2433	399	336
[96, 72]	$((C_4 \times C_4) \rtimes_\varphi C_3) \rtimes_\varphi C_2$	×	×	×	✓	2433	399	336
[96, 73]	$C_8 \times A_4$	✓	×	×	✓	—	—	—
[96, 74]	$((C_8 \times C_2) \rtimes_\varphi C_2) \rtimes_\varphi C_3$	✓✓	✓	✓	×	3884	678	630
[96, 185]	$A_4 \rtimes_\varphi Q_8$	×	×	×	✓	16	0	0
[96, 186]	$C_4 \times S_4$	✓	×	×	✓	113	0	0
[96, 187]	$(C_2 \times S_4) \rtimes_\varphi C_2$	×	×	×	✓	16	0	0
[96, 188]	$\mathrm{SL}(2,3) \rightarrow G \rightarrow C_2)$	✓	×	✓✓	×	14	0	0
[96, 189]	$C_2 \times \mathrm{GL}(2,3)$	✓	×	✓	×	14	0	0
[96, 190]	$(C_2 \times \mathrm{SL}(2,3)) \rtimes_\varphi C_2$	×	×	×	×	16	0	0
[96, 191]	$\mathrm{SL}(2,3) \rightarrow G \rightarrow C_2) \rtimes_\varphi C_2$	×	×	×	×	16	0	0
[96, 192]	$\mathrm{SL}(2,3) \rightarrow G \rightarrow C_2) \rtimes_\varphi C_2$	✓✓	✓	✓	×	14	0	0
[96, 193]	$(\mathrm{SL}(2,3) \rtimes_\varphi C_2) \rtimes_\varphi C_2$	×	×	×	×	16	0	0
[96, 194]	$C_2 \times (A_4 \rtimes_\varphi C_4)$	×	×	×	✓	118	0	0
[96, 195]	$(C_2 \times C_2 \times A_4) \rtimes_\varphi C_2$	×	×	×	✓	16	0	0
[96, 196]	$C_2 \times C_4 \times A_4$	×	×	×	✓	—	—	—
[96, 197]	$D_4 \times A_4$	×	×	×	✓	5202	558	486
[96, 198]	$C_2 \times C_2 \times \mathrm{SL}(2,3)$	×	×	×	×	1347	224	198
[96, 199]	$Q_8 \times A_4$	×	×	×	✓	5187	558	486
[96, 200]	$C_2 \times (\mathrm{SL}(2,3) \rtimes_\varphi C_2)$	✓	×	✓	×	1332	224	198
[96, 201]	$(\mathrm{SL}(2,3) \rtimes_\varphi C_2) \rtimes_\varphi C_2$	×	×	×	×	5202	558	486
[96, 202]	$(C_2 \times \mathrm{SL}(2,3)) \rtimes_\varphi C_2$	×	×	×	×	5202	558	486
[96, 203]	$(C_2 \times C_2 \times Q_8) \rtimes_\varphi C_3$	×	×	×	✓	189	0	0
[96, 204]	$((C_2 \times D_4) \rtimes_\varphi C_2) \rtimes_\varphi C_3$	×	×	×	✓	189	0	0
[96, 226]	$C_2 \times C_2 \times S_4$	×	×	×	✓	42	0	0
[96, 227]	$((C_2 \times C_2 \times C_2 \times C_2) \rtimes_\varphi C_3) \rtimes_\varphi C_2$	×	×	×	✓	0	0	0
[96, 228]	$C_2 \times C_2 \times C_2 \times A_4$	×	×	×	✓	—	—	—
[96, 229]	$C_2 \times ((C_2 \times C_2 \times C_2 \times C_2) \rtimes_\varphi C_3)$	×	×	×	✓	4779	853	720

1. Notation and conventions

Our notation follows the GAP Reference Manual, p. 356 [36], with the following exceptions. We denote the direct product by "×" and the semidirect by $N \rtimes_\varphi K$, where N is normal. Beware that this convention is not unique and that the symbol "$\rtimes_\varphi$" may point the other way. In writing short exact sequences like $\mathbf{1} \rightarrow N \rightarrow G \rightarrow Q \rightarrow \mathbf{1}$, we will omit the leading and trailing trivial groups in order to make our notation more compact.

We denote the dihedral group of a regular n-gon by D_n, and *not* by D_{2n}, as some authors prefer to do. C_n or $\mathbb{Z}_n$ is the cyclic group of order n. S_n and A_n are the symmetric and alternating groups, respectively. Q_4 and Q_8 are the quaternion and octonion groups, respectively. $\mathrm{SL}(n, p)$ is the special linear group over a finite field, i.e. the set of all $n \times n$ matrices with determinant 1 and values from a field of order p.

To facilitate the comparison with the existing literature, we give in Appendix A 3 a nonexhaustive list of alternative names for some of the groups considered in our analysis.

Many of the groups that we consider do not have specific names, and we will refer to them by their GAPIDs. $\mathfrak{G}(m, n)$ will denote the group that is generated in GAP by the command SmallGroup (m, n).

TABLE IV. Some aliases for the groups in Table III. The first and second columns give the GAPID and the group names displayed by GAP, respectively. The third column shows one or more alternative names that are in common use in the physics and mathematics literature. The fourth column, finally, gives a short description of the group, where appropriate.

GAPID	Group	Other names	Description
[12, 3]	A_4	$\Delta(12)$, T	Tetrahedral group
[21, 1]	$C_7 \rtimes_\varphi C_3$	T_7	
[24, 3]	SL(2, 3)	T'	Double cover of A_4
[24, 12]	S_4	$\Delta(24)$, O	Octahedral group
[24, 13]	$C_2 \times A_4$	$\Sigma(24)$	Pyritohedral group
[27, 3]	$(C_3 \times C_3) \rtimes_\varphi C_3$	$\Delta(27)$	
[39, 1]	$C_{13} \rtimes_\varphi C_3$	T_{13}	
[42, 2]	$C_2 \times (C_7 \rtimes_\varphi C_3)$	T_{14}	
[48, 3]	$(C_4 \times C_4) \rtimes_\varphi C_3$	$\Delta(48)$	
[48, 28]	$\mathrm{SL}(2, 3) \rightarrow G \rightarrow C_2$		Double cover of S_4
[54, 8]	$((C_3 \times C_3) \rtimes_\varphi C_3) \rtimes_\varphi C_2$	$\Delta(54)$	
[57, 1]	$C_{19} \rtimes_\varphi C_3$	T_{19}	
[60, 5]	A_5	$\Sigma(60)$, I	Icosahedral group
[63, 3]	$C_3 \times (C_7 \rtimes_\varphi C_3)$	T_{21}	
[75, 2]	$(C_5 \times C_5) \rtimes_\varphi C_3$	$\Delta(75)$	
[78, 2]	$C_2 \times (C_{13} \rtimes_\varphi C_3)$	T_{26}	
[81, 7]	$(C_3 \times C_3 \times C_3) \rtimes_\varphi C_3$	$\Sigma(81)$	
[84, 2]	$C_4 \times (C_7 \rtimes_\varphi C_3)$	T_{28}	
[93, 1]	$C_{31} \rtimes_\varphi C_3$	T_{31}	
[96, 64]	$((C_4 \times C_4) \rtimes_\varphi C_3) \rtimes_\varphi C_2$	$\Delta(96)$	

2. The list of 90 groups

In Table III, we list the 90 groups of order ≤ 100 that have a three-dimensional irreducible representation.

The first column gives the GAPID, which is a label that uniquely identifies the group in GAP. The first number in the square brackets is the order of the group, and the second number simply enumerates different groups of the same order. The GAPIDs of the 14 groups that require more than 60 days of computer time are indicated by a dash in the seventh to ninth columns.

The second column gives the name of the group. If two or more groups by the same name are isomorphic, we list only one. For the conventions we used in naming the groups and for a nonexhaustive compilation of alternative names common in the physics and mathematics literature, see Appendixes A 1 and A 3, respectively.

The third column indicates whether the group G is a subgroup of U(3). If G is in SU(3), a double check mark is shown, otherwise a single one.

The fourth and fifth columns indicate whether G is in U(2) or U(2) $\times$ U(1), respectively (single check mark). If G is in SU(2) or SU(2) $\times$ U(1), respectively, there is a double check mark.

The sixth column indicates whether G contains A_4 as a subgroup.

The seventh column gives the total number of inequivalent models, and the eighth and ninth columns show the number of models that have vacua with mixing angles that lie in the 3σ interval or are tribimaximal, respectively.

3. Alternative names for some small groups

In Table IV we list some alternative names for the groups that we have considered in this publication (cf. Table III). To compile this list, we have made use of Refs. [10–12,22,30,37–39].

APPENDIX B: CONSTRUCTION OF THE GROUPS OF ORDER AT MOST 100

We will first describe how to generate all groups of order ≤ 100 in GAP. Then we will determine which groups have a three-dimensional irrep and/or are a subgroup of U(3) or SU(3). We include this information because there seems to be a clear preference in model building for continuous or discrete subgroups of U(3) or SU(3).

1. Generating the groups

The following lines of code generate the list of all groups of order ≤ 100 using the Small Groups Library [23] in GAP:

```
1  SizeScreen( [ 500, ] );
2  groups := AllSmallGroups([1..100]);;
3  for g in groups do
4  Display(StructureDescription(g));
5  Display(IdGroup(g));
6  chartab := Irr(g);;
7  for i in [1..Size(chartab)] do
8  Print(chartab[i][1], " ");
```

```
9                    od;
10                   Print("\n");
11                   od;
12                   time;
```

These lines can be entered directly at the GAP prompt. In the following we assume that the preceding lines have been saved in a file named smallgroups.gap that is then loaded and automatically executed (see line 1 below):

```
1                    gap > Read("smallgroups.gap");
2                    1
3                    [1, 1]
4                    1
5                    C2
6                    [2, 1]
7                    1 1
8                    C3
9                    [3, 1]
10                   1 1 1
```

We only display the first few lines of output (lines 2–10 above). For each group, there are three lines of output corresponding to lines 4, 5, 8 in the GAP code. For a nontrivial example, see lines 5–7 in the output. Line 5 displays the human-readable name of the group, line 6 gives its GAPID which uniquely identifies the group and which we will use as input for other GAP commands, and line 7 gives the first column of the character table, i.e. the dimensions of the irreps [29].

We find 1048 groups of order ≤ 100 which we list in a separate file that we have made available for download [24]. The first two columns of this list summarize the information we have obtained in this section.

2. Groups that are subgroups of SU(3) or U(3)

Next we determine which of these groups are subgroups of U(3) or SU(3). If a group $\mathfrak{g}$ is (isomorphic to) a subgroup of U(3), there is a one-to-one correspondence between its elements and matrices of U(3). These matrices furnish a three-dimensional *faithful* representation of $\mathfrak{g}$ that is not necessarily irreducible. Conversely, if $\mathfrak{g}$ has a three-dimensional, faithful representation, then $\mathfrak{g}$ is a subgroup of U(3): For finite groups, every representation is equivalent to a unitary representation [29], so the representation matrices are elements of U(3). By faithfulness, the representation ρ is a one-to-one mapping between $\mathfrak{g}$ and the image of ρ in U(3). By virtue of ρ being a group homomorphism, Imρ inherits the group properties from $\mathfrak{g}$, and consequently Im$\rho \subset$ U(3) is a group that is isomorphic to $\mathfrak{g}$. Finally, whether $\mathfrak{g}$ lies in SU(3) can be verified by checking the determinant of representation matrices, since equivalent representations have the same determinant.

The kernel of the representation is given by Ker$\rho = \{g \in \mathfrak{g} | \text{char}(g) = \text{char}(1)\}$ [40], and thus a three-dimensional representation ρ is faithful, iff $\mathbb{1}$ is the only element whose character is 3. For each of the 1048 groups generated in Appendix B 1, we calculate the character table. Below is the output for A_4:

```
1                    gap > g := SmallGroup(12, 3);;
2                    gap > Display(StructureDescription(g));
3                    A4
4                    gap > chartab := Irr(g);;
5                    gap > Display(chartab);
6                    [ [ 1, 1, 1, 1 ],
7                    [ 1, E(3)^2, 1, E(3) ],
8                    [1, E(3), 1, E(3)^2],
9                    [3, 0, −1, 0]]
```

On line 1, we specify the group by entering its GAPID [12,3]; see Table III. Lines 6–9 give its character table, where $\mathrm{E}(3) = \exp 2\pi i/3$ denotes the primitive third root of unity. The first column gives the dimensions of the representations: **1**, **1**′, **1**″, **3**. On line 9 corresponding to **3**, there is only one character equal to 3, so **3** is faithful. This proves that A_4 is a subgroup of U(3). The representation matrices can be found by using the REPSN package [41] in GAP:

```
1    gap > LoadPackage(repsn);;
2    gap > for i in[1..Size(chartab)]do
3    >Display(IrreducibleAffordingRepresentation(chartab[i]));
4    >od;
5    Pcgs([f1, f2, f3]) − >[[[1]], [[1]], [[1]]]
6    Pcgs([f1, f2, f3]) − >[[[E(3)^2]], [[1]], [[1]]]
7    Pcgs([f1, f2, f3]) − >[[[E(3)]], [[1]], [[1]]]
8    Pcgs([f1, f2, f3]) − >[[[0, 1, 0], [0, 0, 1], [1, 0, 0]],
9    [[−1, 0, 0], [0, 1, 0], [0, 0, −1]],
10   [[−1, 0, 0], [0, −1, 0], [0, 0, 1]]]
```

Lines 8, 9, 10, respectively, correspond to the representation matrices of the generators f1, f2, f3 of A_4 for the three-dimensional irrep. Their determinants are all 1, and thus A_4 is a subgroup of SU(3).

In other cases, when there is no faithful, irreducible three-dimensional representation, we have to consider the reducible ones. If A, B are two representations, then $\text{char}(A \oplus B) = \text{char}(A) + \text{char}(B)$; i.e. we obtain the character of $A \oplus B$ by adding the rows in the character table that correspond to A and B. For a given group, we consider all direct sums that are three dimensional and calculate their characters. For each direct sum, the first element of the character will be 3, corresponding to the dimension of the representation. If there is more than one 3, we conclude that the direct sum is not faithful. If we cannot find any direct sum that is faithful, we conclude that $\mathfrak{g}$ is not isomorphic to a subgroup of U(3).

Assume that we can find a three-dimensional faithful, reducible representation, thereby proving that $\mathfrak{g}$ is a subgroup of U(3). The representation matrices are block diagonal, and each submatrix is unitary. There are two cases: All submatrices are 1×1, or one is 2×2 and the other is 1×1. In the former case, the representation

matrices are diagonal and commute; thus $\mathfrak{g} \simeq \mathbb{Z}_p \times \mathbb{Z}_q \times \mathbb{Z}_r \subset \mathrm{U}(1)^n$ for some $n \leq 3$. In the latter case, we consider the canonical embedding of the submatrices into U(3) (i.e. by extending the submatrix by the identity matrix to match the dimensions). Every representation matrix can be uniquely written as a product of these embedded submatrices, and the submatrices corresponding to different blocks trivially commute. This establishes that $\mathfrak{g}$ is isomorphic to a subgroup of $\mathrm{U}(2) \times \mathrm{U}(1)$.

We have implemented the above algorithm in a GAP script. The results have been summarized in Ref. [24] and made available for download.

3. Comparing our results to the existing literature

We have compared our results to the existing literature on SU(3) subgroups [12,22,30,37–39]. Identifying the groups is not always straightforward, since they may appear under different names in different contexts; e.g. A_4 is listed as $\Delta(12)$ in Ref. [38] and as part of the C series in Ref. [37].

In Table 1 of Ref. [24] we list all groups of order at most 100 and for each group indicate whether it is a subgroup of U(3), SU(3), U(2), SU(2), $\mathrm{U}(2) \times \mathrm{U}(1)$, or $\mathrm{SU}(2) \times \mathrm{U}(1)$, respectively.

We find that the groups in our list that are subgroups of SU(3) but not of $\mathrm{U}(2) \times \mathrm{U}(1)$ agree with those in Refs. [30,38,39] except in the following cases: According to Ref. [30], the groups $\mathfrak{G}(42, 2)$, $\mathfrak{G}(78, 2)$, $\mathfrak{G}(84, 2)$ are in SU(3), but our analysis along the lines of Appendix B 2 shows that they are only in U(3), not in SU(3).

Reference [12] only explicitly lists groups that are not direct products with cyclic factors, and thus does not consider the groups in question, but according to Theorem II.2 in the same publication, these groups are in U(3), so we have agreement.

Also, the groups $\mathfrak{G}(36, 11)$, $\mathfrak{G}(72, 42)$, $\mathfrak{G}(81, 9)$, and $\mathfrak{G}(84, 11)$ were not listed in Refs. [30,38,39], but we have verified that these groups are indeed in SU(3). $\mathfrak{G}(81, 9)$ and $\mathfrak{G}(84, 11)$ are part of the C series as given in Ref. [37]. This has already been pointed out by Ref. [12]. The groups $\mathfrak{G}(36, 11)$ and $\mathfrak{G}(72, 42)$ have not been explicitly listed in Ref. [12], but the discussion following Theorem II.2 in the same publication makes it clear that these groups are in SU(3).

Reference [12], Sec. II.1, makes the observation that a finite subgroup of U(3) is not in U(2) or U(1), if and only if it has a faithful three-dimensional irreducible representation. In our analysis, we find counterexamples: For instance, the group $\mathfrak{G}(16, 3) \subset \mathrm{U}(3)$ is not in U(2) and has no three-dimensional irreducible representation. The reason is that the existence of a *reducible and faithful* three-dimensional representation is already sufficient for being a subgroup of U(3). For more details, see Appendix B 2.

For generating the $\Delta(3n^2)$ series, we have used the generators from Table 1 in Ref. [38] with $j = 1$ and $k = 0$ (also see Ref. [42]). Note that if we take some arbitrary integers j and k, the representation may not be faithful and thus will not generate [a subgroup of U(3) that is isomorphic to] $\Delta(3n^2)$. Also note that in Ref. [38] the generators for $\Sigma(360)$ generate a group of order 1080 which is a nonsplit extension[1] of A_6 by C_3, and not A_6. We agree with Ref. [37], which lists the same group as $\Sigma(360\phi)$.

4. Groups that contain A_4 as a subgroup

Since many publications in the past have highlighted A_4 and its connection to tribimaximal mixing, we find it useful to list the groups that contain A_4 as a subgroup:

```
1   LoadPackage(“sonata”);
2   for n in [1..100] do
3   for g in AllSmallGroups(n) do
4   sg := Subgroups(g);
5   if "A4" in List(sg, x − >StructureDescription(x)) then
6   Print(IdGroup(g),“\n”);
7   fi;
8   od;
9   UnloadSmallGroupsData();
10  od;
```

For every n from 1 to 100 (line 2), we generate all groups of order n (line 3). For each such group, we determine its subgroups (line 4) and check whether A_4 is one of them (line 5). If the answer is positive, we print the GAPID of the respective group (line 6). On a technical note, since the number of subgroups becomes large, we need to increase the default memory allocation for GAP. The results are presented in the last column of Table 1 in Ref. [24].

APPENDIX C: CLEBSCH-GORDAN COEFFICIENTS FOR FINITE GROUPS

Currently, it is general practice to construct the CGCs for the various groups that are studied in physics on a case-by-case basis using heuristic methods. It is clear that such an approach becomes cumbersome, if one considers more than one group or if the number of irreducible representations is large. Also, for automating the steps from the choice of the family symmetry to finding the invariant Lagrangian to calculating the mixing angles and phases, we need a systematic way of deriving the CGCs that does not rely on the specifics of the group under consideration.

An algorithm due to van den Broek and Cornwell [25] solves this problem in full generality: Given the character table and the explicit form of the unitary representation

[1]We are indebted to Patrick Otto Ludl for pointing out that it is not the direct product of A_6 and C_3 as we had incorrectly identified in the first version of this publication due to a misinterpretation of the GAP output.

matrices, it calculates the CGCs for any finite group. We have implemented this algorithm in PYTHON to automatically generate the CGCs for any finite group. We get the character table and the representation matrices from GAP that we have interfaced with our PYTHON programs to achieve a high level of automation.

We performed several checks to ascertain that the CGCs are calculated correctly. For one thing, we have compared our output to the (comparatively few) results that exist in the literature (see Ref. [22] and references therein). For another, we have checked, for all 90 groups in Table III and for all irreducible representations $\boldsymbol{p}$, $\boldsymbol{q}$, that contractions with the CGCs, namely, $C_{ijk}\boldsymbol{p}_i\boldsymbol{q}_j$, transform like the terms on the right-hand side of the tensor product decomposition $\boldsymbol{p} \otimes \boldsymbol{q}$ (note that this is the defining property for CGCs).

We find complete agreement except for A_5. The problem can be traced back to the fact that the representation matrices for A_5 provided by GAP are not unitary. After choosing unitary representation matrices, the algorithm also gives the correct CGCs for this remaining case.

[1] Y. Fukuda *et al.* (Super-Kamiokande Collaboration), Phys. Rev. Lett. **81**, 1562 (1998).
[2] Q. R. Ahmad *et al.* (SNO Collaboration), Phys. Rev. Lett. **89**, 011301 (2002).
[3] B. Pontecorvo, Sov. Phys. JETP **6**, 429 (1957).
[4] Z. Maki, M. Nakagawa, and S. Sakata, Prog. Theor. Phys. **28**, 870 (1962).
[5] T. Schwetz, M. A. Tortola, and J. W. F. Valle, New J. Phys. **10**, 113011 (2008).
[6] M. C. Gonzalez-Garcia, M. Maltoni, and J. Salvado, J. High Energy Phys. 04 (2010) 056.
[7] M. Kobayashi and T. Maskawa, Prog. Theor. Phys. **49**, 652 (1973).
[8] P. F. Harrison, D. H. Perkins, and W. G. Scott, Phys. Lett. B **530**, 167 (2002).
[9] P. F. Harrison and W. G. Scott, Phys. Lett. B **535**, 163 (2002).
[10] G. Altarelli and F. Feruglio, Rev. Mod. Phys. **82**, 2701 (2010).
[11] H. Ishimori *et al.*, Prog. Theor. Phys. Suppl. **183**, 1 (2010).
[12] P. O. Ludl, J. Phys. A **43**, 395204 (2010); **44**, 139501(E) (2011).
[13] E. Ma and G. Rajasekaran, Phys. Rev. D **64**, 113012 (2001).
[14] E. Ma, arXiv:hep-ph/0409075.
[15] K. S. Babu and X.-G. He, arXiv:hep-ph/0507217.
[16] G. Altarelli and F. Feruglio, Nucl. Phys. **B741**, 215 (2006).
[17] M. Mezzetto and T. Schwetz, J. Phys. G **37**, 103001 (2010).
[18] G. L. Fogli, E. Lisi, A. Marrone, A. Palazzo, and A. M. Rotunno, J. Phys. Conf. Ser. **203**, 012103 (2010).
[19] Y. Kajiyama and H. Okada, Nucl. Phys. **B848**, 303 (2011).
[20] F. Plentinger, G. Seidl, and W. Winter, J. High Energy Phys. 04 (2008) 077.
[21] The GAP Group, "GAP—Groups, Algorithms, and Programming, Version 4.4.12," http://www.gap-system.org, 2008.
[22] P. O. Ludl, arXiv:0907.5587.
[23] B. E. Hans Ulrich Besche and E. O'Brien, "Small Groups—A GAP package" http://www.icm.tu-bs.de/~beick/soft/small/small.html.
[24] See Supplementary Material at http://link.aps.org/supplemental/10.1103/PhysRevD.84.013011 for the full list of the 1048 groups of order at most 100.
[25] P. van den Broek and J. Cornwell, Phys. Status Solidi B **90**, 211 (1978).
[26] K. Nakamura and P. D. Group, J. Phys. G **37**, 075021 (2010).
[27] S. M. Bilenky, J. Hosek, and S. T. Petcov, Phys. Lett. **94B**, 495 (1980).
[28] F. Plentinger, G. Seidl, and W. Winter, Nucl. Phys. **B791**, 60 (2008).
[29] H. F. Jones, *Groups, Representations and Physics* (Hilger, Bristol, England, 1990), p. 287.
[30] W. M. Fairbairn and T. Fulton, J. Math. Phys. (N.Y.) **23**, 1747 (1982).
[31] C. Luhn, S. Nasri, and P. Ramond, Phys. Lett. B **652**, 27 (2007).
[32] C. Hagedorn, M. A. Schmidt, and A. Y. Smirnov, Phys. Rev. D **79**, 036002 (2009).
[33] Q.-H. Cao, S. Khalil, E. Ma, and H. Okada, Phys. Rev. Lett. **106**, 131801 (2011).
[34] See Supplementary Material at http://link.aps.org/supplemental/10.1103/PhysRevD.84.013011 for the graphs of all 67 flavor groups that have nonsingular mass matrices.
[35] S. Lang, *Algebra* (Springer, Heidelberg, 2002).
[36] The GAP Group, "GAP Reference Manual," http://www.gap-system.org/Manuals/doc/ref/manual.pdf, 2008.
[37] G. A. Miller, H. F. Blichfeldt, and L. E. Dickson, *Theory and Applications of Finite Groups* (Dover, New York, 1961).
[38] W. M. Fairbairn, T. Fulton, and W. H. Klink, J. Math. Phys. (N.Y.) **5**, 1038 (1964).
[39] A. Bovier, M. Luling, and D. Wyler, J. Math. Phys. (N.Y.) **22**, 1543 (1981).
[40] I. M. Isaacs, *Character Theory of Finite Groups* (Academic Press, New York, 1976).
[41] V. Dabbaghian, "Repsn—A GAP package," http://www.sfu.ca/~vdabbagh/gap/repsn.html.
[42] C. Luhn, S. Nasri, and P. Ramond, J. Math. Phys. (N.Y.) **48**, 073501 (2007).